Application of TiO2 Fusiform Nanorods for Dye-Sensitized Solar Cells with Significantly Improved Efficiency

ARTICLE *in* THE JOURNAL OF PHYSICAL CHEMISTRY C · AUGUST 2011

Impact Factor: 4.77 · DOI: 10.1021/jp204725f

5 AUTHORS, INCLUDING:

Ke Fan
KTH Royal Institute of Technology
34 PUBLICATIONS **573** CITATIONS
SEE PROFILE

Tianyou Peng
Wuhan University
214 PUBLICATIONS **5,217** CITATIONS
SEE PROFILE

THE JOURNAL OF PHYSICAL CHEMISTRY C

ARTICLE

pubs.acs.org/JPCC

Application of TiO_2 Fusiform Nanorods for Dye-Sensitized Solar Cells with Significantly Improved Efficiency

Ke Fan, Wei Zhang, Tianyou Peng,* Junnian Chen, and Fan Yang

College of Chemistry and Molecular Science, Wuhan University, Wuhan 430072, People's Republic of China

ABSTRACT: Anatase TiO_2 fusiform nanorods with diameters 20−80 nm and lengths 200−400 nm are synthesized by a two-step hydrothermal method, and the effects of the obtained TiO_2 nanorod content in a P25-based electrode on the performances of dye-sensitized solar cell were investigated by using photocurrent−voltage, open-circuit voltage decay and electrochemical impedance spectroscopy measurements. The results show that those fusiform TiO_2 nanorods in the P25-based electrode not only provide a straight path for the electron transport but also function as scattering particles to increase light harvesting efficiency of the solar cell, and the optimal conversion efficiency of 4.68% is obtained from a solar cell fabricated with a P25-based electrode containing 10 wt % nanorods, with a 66.5% improvement in the efficiency with lower resistance and longer electron lifetimes as compared to the bare P25-based solar cell. This should be attributed to the reduced charge recombination and the sufficient scattering effect of the nanorods in the film electrode.

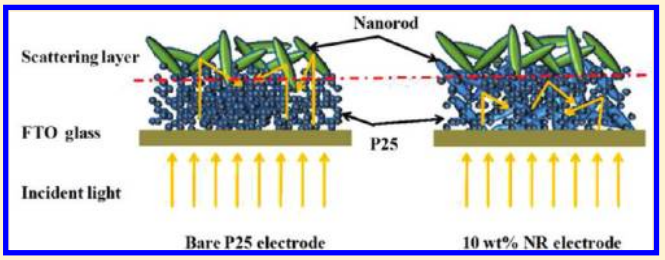

1. INTRODUCTION

Dye-sensitized solar cells (DSSCs) have promoted intense research in the decades due to their low cost, highly efficient conversion of visible light into electricity, and eco-friendly production.[1] Compared to the conventional silicon devices, DSSCs hold the promise of lower fabrication cost and have efficiency comparable to the amorphous silicon solar cells. Generally, DSSCs are mainly composed of three parts: the dye-sensitized nanocrystal film as photoanode, the redox couple (usually I_3^-/I^-) in organic solvent(s), and the platinized transparent conducting oxide (TCO) glass as the counter electrode. Among those, the photoanode usually consists of porous TiO_2 film adsorbed by dye molecules (such as a ruthenium complex), which can absorb the light energy, especially the visible light of sunshine. The dye molecules move to the excited states when the DSSC is exposed to light irradiation with suitable energy, and the excited-state electrons are injected quickly into the conduction band of TiO_2; these injected electrons are collected through the conducting substrate of the TiO_2 photoanode. The dye molecules can be regenerated by the iodide ions in the electrolyte, and then the resulting triiodide ions can accept electrons from the platinized TCO counter electrode to fulfill a complete current cycle in DSSCs.[1]

Although the best conversion efficiency of DSSC has exceeded 10% up until now,[2] there would be a lot of surface traps on the TiO_2 nanopaticles in the film electrode, resulting in serious charge recombination during the electron transfer between TiO_2 nanoparticles or from electrolyte to TiO_2, which slows the electron transport rate and limits the performance of the cell.[3] Fabrication of film electrodes from one-dimensional nanostructured material has proven to be an effective way to facilitate electron transport. Some one-dimensional TiO_2 such as nanowires,[4−6] nanotubes,[7−10] and nanofibers,[11,12] have been synthesized and applied in DSSCs. Compared with conditional TiO_2 nanoparticles, these one-dimensional structures can supply a straight path for the electron transfer and improve the electron mobility and transport rate to reduce the recombination significantly. However, the dye adsorption on these one-dimensional TiO_2 is often insufficient because of its relatively large particle size and small surface area. Another challenge is the poor harvesting efficiency of solar light with wavelengths longer than 600 nm, due to the transmission of incident light through the TiO_2 photoanode. One way to enhance the light harvesting is to synthesize hierarchically structured photoelectrodes (mesoporous spheres for example) for dye-sensitized solar cells,[13] another way is using scattering layer. Additional scattering layers made of large TiO_2 particles, usually 100−400 nm diameter, have been coated onto the photoanodes to improve the light absorbance. Due to the relatively large diameter, the scattering particles would reflect the transmissible incident light through the TiO_2 photoanode to compensate for the loss of light harvesting and therefore improve the performance of cells.[14−16]

Herein, anatase TiO_2 fusiform nanorods (NR) with diameters 20−80 nm and lengths 200−400 nm were synthesized by a two-step hydrothermal method. The composites of nanorods and commercial TiO_2 nanoparticles (P25) were used to fabricate the photoanodes for DSSCs. The effects of the weight content of the fusiform nanorods on the performance of the solar cells were investigated, and the optimal ratio should be containing 10 wt % nanorods in the TiO_2 electrode. Additionally, it is found that it is not necessary to add scattering particles to the electrode containing 10 wt % nanorods, indicating the synthesized nanorods can

Received: May 21, 2011
Revised: July 16, 2011
Published: July 29, 2011

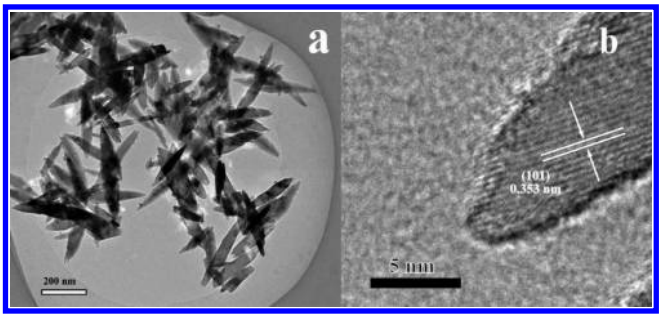

Figure 1. TEM and HRTEM images of the obtained TiO_2 nanorods by using P25 as the precursor.

not only reduce the charge recombination but also provide scattering effect to improve the light harvesting.

2. EXPERIMENTAL SECTION

2.1. Preparation of TiO_2 Fusiform Nanorods. TiO_2 fusiform nanorods were prepared by a two-step hydrothermal synthesis.[17] Briefly, 175 g of TiO_2 powder (P25, Degussa AG, Germany), which consists of about 30% rutile and 70% anatase and a primary particle size of about 21 nm, was mixed with 70 mL of 10 M NaOH solution, followed by treating the mixture at 130 °C in a Teflon-lined autoclave for 20 h. After the hydrothermal treatment, the sample was washed with 0.1 M HNO_3 solution to give a suspension (100 mL) of pH 5.6, which was subjected to the second hydrothermal treatment in the autoclave at 175 °C for 48 h. The resulting slurries were then filtered and dried at 100 °C for 3 h to give the final products.

2.2. Preparation of Photoanodes. A 1.0 g portion of TiO_2 containing different weight ratios of the obtained TiO_2 nanorods/P25 was mixed with 8.0 mL of ethanol, 0.2 mL of acetic acid, 3.0 g of terpinol and 0.5 g of ethyl cellulose by ball-milling for 10 h. The obtained paste was spread on a clean FTO glass (15 Ω/sq) by using the doctor blading technique. The thicknesses of the films were controlled by adhesive tape (Scotch, 50 μm) serving as spacers. After drying in atmosphere, the film was sintered at 500 °C for 1 h to remove the binders in the paste. As for the scattering layer by using the obtained TiO_2 nanorods, a bare nanorod paste was spread on the same electrode as the above one and was sintered at 500 °C for 1 h again. Dye sensitization was achieved by immersing the electrodes with and without nanorod scattering layer in a 0.3 mM N719 dye (Solaronix) in ethanol solution overnight, followed by rinsing in ethanol and drying in air.

2.3. Fabrication of DSSCs. The dye-sensitized electrode was assembled in a typical sandwich-type cell; the identical platinized FTO counter electrode was placed over the dye-sensitized electrode, and the electrolyte, containing 0.5 M LiI, 0.05 M I_2, and 0.1 M 4-*tert*-butylpyridine in 1:1 acetonitrile propylene carbonate, was sandwiched between the photoanode and the platinized counter electrode by firm press. Adhesive tape (approximately 50 μm) was placed between the photoanode and the counter electrode to avoid short-circuiting.

2.4. TiO_2 Nanorod Characterization and Photoelectrochemical Measurements of Electrodes. Structure phase analyses with X-ray diffraction (XRD) method were performed on a D_8-advance X-ray diffractometer (Bruker) with Cu Kα radiation (λ = 0.15418 nm). The microstructures were explored by a high-resolution transmission electron microscope (HRTEM; JEM2100F).

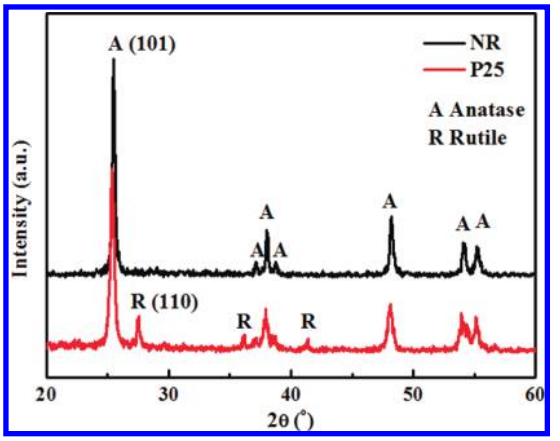

Figure 2. XRD patterns of P25 and the prepared TiO_2 nanorods.

The morphologies of the films were investigated by scanning electron microscope (SEM; JSM-6700F). The pore-size distributions of different films was obtained using a nitrogen adsorption apparatus (Micrometrics ASAP 2010).

To estimate the dye adsorbed amount on the TiO_2 films, the sensitized electrode was separately immersed into a 0.1 M NaOH solution in a mixed solvent (water:ethanol = 1:1), which resulted in the desorption of N719. The absorbance of the resulting solution was measured by a UV-3600 UV−vis spectrophotometer (Shimadzu, Japan). The dye adsorbed amount was determined by the molar extinction coefficient of 1.41×10^4 dm^3 mol^{-1} cm^{-1} at 515 nm as reported previously.[18]

The DSSC was illuminated by light with energy of 100 mW cm^{-2} (AM 1.5) from a 300 W solar simulator (Newport, 91160). The light intensity was determined using a SRC-1000-TC-QZ-N reference monocrystalline silicon cell system (Oriel, U.S.). Computer-controlled Keithley 2400 sourcemeter was employed to collect the photocurrent−voltage ($J-V$) curves of DSSCs. The active area was 0.25 cm^2.

The electrochemical impedance spectroscopy (EIS) measurements were carried out by applying bias of the open-circuit voltage (V_{OC}) without electric current under 100 mW cm^{-2} illumination and were recorded over a frequency range of 0.05−10^5 Hz with ac amplitude of 10 mV. For the photoinduced open circuit voltage decay (OCVD) measurements, the illumination was turned off using a shutter after the cell was first illuminated to a steady voltage, and then the OCVD curve was recorded. The above measurements were carried out on a CHI-604C electrochemical analyzer.

The photon to electricity conversion efficiency was calculated according to eq 1

$$\eta(\%) = \frac{V_{OC} J_{SC} FF}{P_{in}} \times 100 \quad (1)$$

where η is the overall energy conversion efficiency and V_{OC}, J_{SC}, and FF are the open-circuit photovoltage, the short-circuit photocurrent density, and the fill factor, respectively. P_{in} is the energy of the incident light (100 mW cm^{-2}).

3. RESULTS AND DISCUSSION

3.1. Crystal Phase and Morphology Analyses. Figure 1 shows the TEM and HRTEM images of the obtained TiO_2 nanorods. As can be seen in Figure 1a, fusiform nanorods with

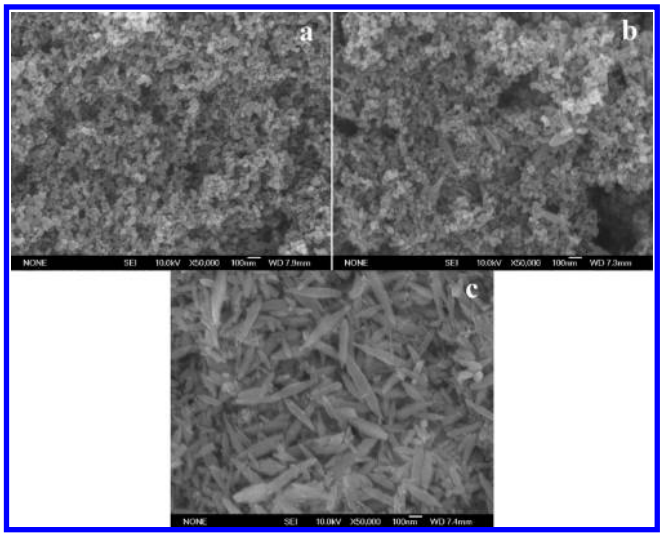

Figure 3. SEM images of electrodes with bare P25 (a), 10 wt % nanorods (b), and bare nanorods (c).

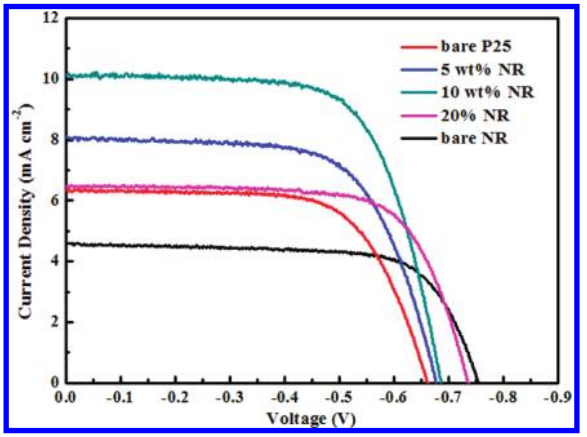

Figure 4. Photocurrent−voltage ($J-V$) curves of DSSCs fabricated with the P25-based electrodes containing different nanorod contents.

diameter 20−80 nm and length of 200−400 nm were obtained via the two-step hydrothermal treatment of P25 nanoparticles. Figure 1b presents the HRTEM image of the obtained TiO_2 nanorods. The lattice fringes with interplanar distances of 0.353 nm, which are in good agreement with the *d* spacing values of the anatase (101) planes, can be observed clearly in the HRTEM image. Figure 2 depicts the XRD patterns of P25 as the precursor and the obtained nanorods. It is clear that the crystal phase of the final product derived from the hydrothermal method is anatase (JCPDS 73-1764). The main peak of rutile (110) plane of P25 totally disappeared after the two-step hydrothermal treatment, indicating the 30% rutile in P25 has been converted to anatase TiO_2. The above HRTEM image and XRD pattern indicate the producted nanorods should be anatase crystal phase. As for the application of the nanorods in the DSSCs, the anatase phase is more favorable for photoresponse than the rutile one,[19] and therefore, it could be expected that the present anatase TiO_2 nanorods should improve the performances of the P25-based DSSCs, which will be further discussed in the following sections. Panels a−c of Figure 3 show the SEM images of films consist of bare P25, 10 wt % nanorods, and bare nanorods respectively.

Table 1. The Photovoltaic Performances of the Recombination Reactions within the DSSCs Fabricated with Different Electrodes

electrode	V_{oc} (V)	J_{sc} (mA cm^{-2})	FF	η (%)
bare P25	0.660	6.32	0.67	2.81
5 wt % NR	0.676	8.06	0.66	3.51
10 wt % NR	0.686	10.13	0.57	4.68
20 wt % NR	0.735	6.48	0.70	3.35
bare NR	0.754	4.56	0.71	2.45

In Figure 3a, it is observed that the film of bare P25 particles is homogeneous and good interconnection is formed between particles. In panels b and c of Figure 3, which shows 10 wt % nanorod electrode and bare TiO_2 nanorods, respectively, some fragments from nanorods exist in the films. This is mainly due to the ball-milling process for the preparation of the electrode, whose strongly mechanical shear force would result in part of the nanorods fragmenting into smaller ones.

3.2. Photovoltaic Performance. Figure 4 shows the $J-V$ curves of DSSCs fabricated with the P25-based electrodes containing different weight contents of the obtained nanorods. The values of V_{OC}, J_{SC}, FF, and conversion efficiencies (η) of the electrodes are shown in Table 1. Apparently, the nanorod content in the P25-based electrode contributes a significant influence on the performances of the solar cell. All DSSCs fabricated with electrodes containing the obtained nanorods display higher V_{OC} as compared to the solar cell based on a bare P25 electrode. Furthermore, V_{OC} is improved from 0.66 to 0.75 V with enhancing the nanorod weight content in the P25-based electrode from 0 to 100%. Generally, V_{OC} of a solar cell is determined by the difference between the Fermi level for electrons in the TiO_2 electrode and the redox potential of I_3^-/I^-. Due to the one-dimensional structure of the present nanorods, the charge recombination could decrease and charge transfer rate increases because of its straight charge transfer path divided by the nanorods, which result in an increase of electron density in TiO_2 electrode, and thus the positive shift of Fermi level. What is more, it is reasonable to think the relatively larger size of the present nanorods than P25 could enlarge the pore size of the film to improve the diffusion of liquid electrolyte, which is beneficial for electron transfer in I_3^-/I^- electrolyte.[20] The above-mentioned low electron recombination and fast electrolyte diffusion are beneficial for lowering the concentration of I_3^-,[21] and the V_{OC} depends logarithmically on the inverse concentration of I_3^-.[21] Consequently, the V_{OC} increases with enhancing the nanorod weight content in the P25-based electrodes.

As can be seen in Table 1, J_{SC} shows an increasing behavior first from 6.32 to 10.13 mA cm^{-2} when the nanorod content is less than 10 wt %. Once the nanorod content exceeds 10 wt %, J_{SC} starts to drop dramatically from 10.13 to 4.56 mA cm^{-2}. The dependence of η on the nanorod content is consistent with that of J_{SC}, which achieves the maximum energy conversion efficiency 4.68% at the 10 wt % nanorod and then decreases when the nanorod content is beyond 10 wt %. Apparently the performance of DSSCs in our case is more dependent on J_{SC} behavior than other factors. Compared with the efficiency 2.81% of solar cell fabricated with bare P25-based electrode, the optimized DSSC containing 10 wt % TiO_2 nanorods increases the efficiency significantly by 66.5%.

The behavior of DSSCs with different content of TiO_2 nanorods is understandable as follows. As shown in Figure 5, the dye adsorption of TiO_2 electrodes reduced from 3.72×10^{-8} to 1.78×10^{-8} mol cm^{-2} with the nanorod content enhancing from 0 to 100 wt %. Although the present one-dimensional structure of nanorods could reduce the charge recombination and accelerate the charge transfer rate in the TiO_2 film due to the low surface traps, the relatively low specific surface area leads to decreases in the dye adsorption of TiO_2 film, which leads to less photon excited electrons injected to TiO_2 conduction band and then to the decreased photocurrrent. As a result, J_{SC} achieved the maximum at the TiO_2 electrodes containing 10 wt % nanorods. Consequently, the DSSC with the best performance should contain 10 wt % nanorods after optimization as shown in Table 1.

3.3. Photoelectrochemical Behavior Analyses. To further understand the effects of TiO_2 nanorods on the performance of the P25-based cell, the EIS spectra of DSSCs fabricated with P25-based electrode containg 10 wt % nanorods, the bare P25, and bare nanorods electrodes were carried out, and their Nyquist and Bode plots are shown in panels a and b of Figure 6, respectively. Typically, the Nyquist diagram features three semicircles that in the order of increasing frequency are attributed to the Nernst diffusion within the electrolyte, the electron transfer at the TiO_2/electrolyte interface, and the redox reaction at the platinum counter electrode.[22] Accordingly, there should be three peaks in Bode plots. In our case, two main semicircles appear in Nyquist plots, and the semicircle attributed to the Nernst diffusion does not present due to the relatively fast diffusion of the electrolyte in the TiO_2 films.[23] The electron lifetime (τ_n) can be drawn by the position of the low frequency peak in Figure 6b through $\tau_n = 1/2\pi f$ (f means the frequency of superimposed ac voltage).[24]

The size of the semicircle at low frequency becomes much smaller after mixing 10 wt % nanorod in the electrode as compared to the bare P25 electrode as shown in Figure 6a, indicating a lower resistance of the electron transfer at the TiO_2/electrolyte interface. As mentioned above, nanorods in the film electrode could reduce the charge recombination and promote the electron transfer because of their one-dimensional structure. Furthermore, as shown in Figure 7, the content of nanorod is critical to the pore-size distribution of the film. The main pore widths of bare P25, 10 wt % nanorod, and bare nanorod electrode are 42.9, 51.5, and 59.7 nm, respectively. Obviously, due to its relatively large particle size, a nanorod would lead to the enlarged pore size of the film, which could improve the diffusion of liquid electrolyte. All of these can decrease the resistance of electron transfer at the TiO_2/electrolyte interface, resulting in smaller semicircles at low frequency. It is also noted that the contact resistance (the initial point of the Nyquist plots) of the bare P25, 10 wt % nanorod, and bare nanorod film is 18.80, 14.36, and 15.85 Ω, respectively. It seems there appears to be a decrease in the contact resistance for the 10% nanorod film and bare nanorod

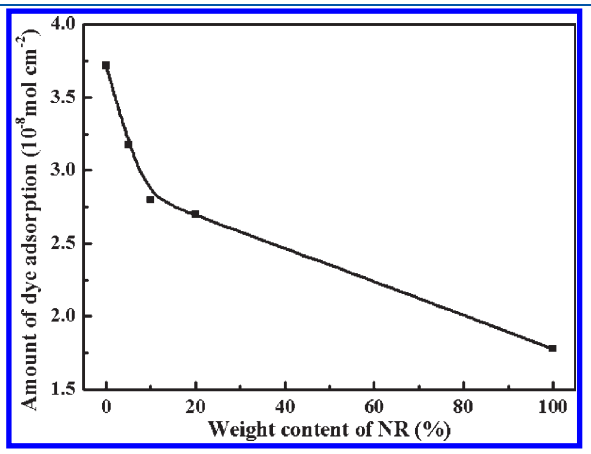

Figure 5. Dye adsorption amount of TiO_2 electrodes containing different TiO_2 nanorods.

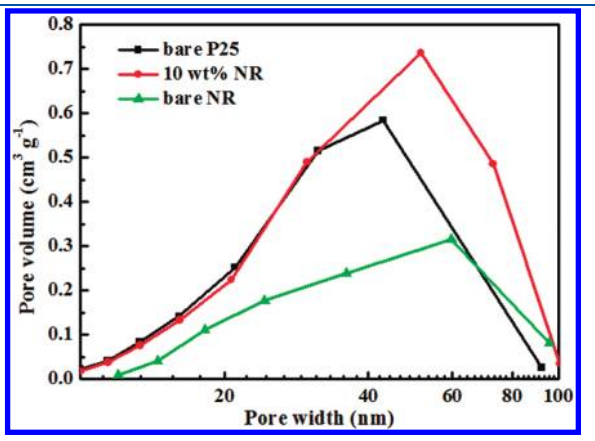

Figure 7. Pore-size distribution of the composite electrode containing 10 wt % nanorods, the bare P25, and nanorod electrodes.

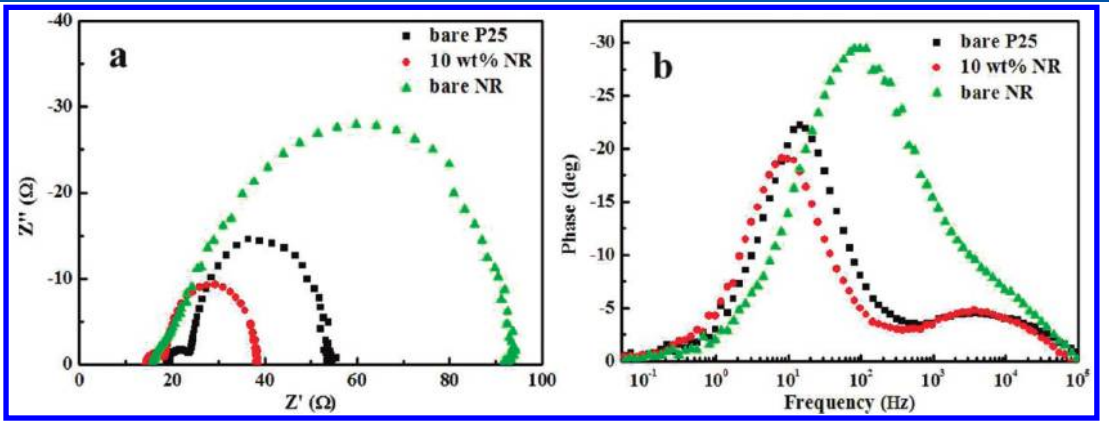

Figure 6. Electrochemical impedance spectroscopy (EIS) of DSSCs fabricated with the composite electrode containing 10 wt % nanorods, the bare P25, and nanorod electrodes: a, Nyquist plots; b, Bode plots.

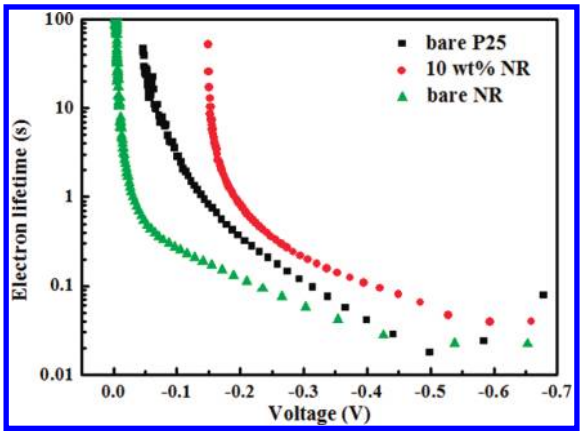

Figure 8. Open-circuit voltage decay (OCVD) curves of DSSCs fabricated with the composite electrode containing 10 wt % nanorods, the bare P25, and nanorod electrodes.

film. It is well-known that the contact resistance of the DSSC is influenced by the sheet resistances of the substrate as well as the redox species diffusion in the electrolyte.[25,26] All the cells have the same FTO−glass substrate; therefore, it can be concluded that the decrease in the contact resistance for the 10% NR film and bare NR film should be attributed to the enhanced electrolyte diffusion, which results from the enlarged pore size of the films.

However, the bare nanorod electrode displays a much lager semicircle at low frequency, even larger than that of the bare P25 electrode. This should be owing to its poor dye absorption as shown in Figure 5. Accordingly, the peaks of electrodes at low frequency containing 10 wt % nanorods and bare nanorods in Bode plots shift to lower position and higher position as compared to the bare P25 electrode, respectively. The above results indicate that electrode lifetime in the composite electrode containing 10 wt % nanorods (16.3 ms) is longer than these of the bare nanorod (1.6 ms) and bare P25 electrode (11.1 ms).

The open-circuit voltage decay (OCVD) curves can show more detailed information of the interfacial recombination processes between the photoinjected electrons in the TiO_2 electrode and electrolyte under the dark state.[27] Under the present open-circuit and dark state conditions, the electron transport resistance in the TiO_2 film does not affect the OCVD measurements because there is no current flow through the cell, and the electron lifetime (τ'_n) in DSSCs can change with the cell's open circuit voltage (V_{OC}) due to the shift of semiconductor's Fermi level.[27] Therefore, the effects of the electron traps on the recombination reaction can be qualitatively explained by analyzing the shapes of $\tau'_n \sim V_{OC}$ relation curves. The electron lifetime (τ'_n) can be derived from the OCVD measurements according to eq 2

$$\tau'_n = -\frac{k_B T}{e}\left(\frac{dV_{OC}}{dt}\right)^{-1} \quad (2)$$

where k_B is the Boltzmann constant, T is the temperature, and e is the electron charge.

Figure 8 shows the $\tau'_n \sim V_{OC}$ relation curves of cells fabricated with composite electrode containing 10 wt % nanorods, the bare P25, and nanorod electrodes. As shown in Figure 8, the electron lifetimes (τ'_n) show an exponential dependence at the V_{OC} and make a good agreement with the result obtained from EIS measurement, from which a 10 wt % nanorod electrode has the longest electron lifetime and the bare nanorod electrode has the shortest one. This phenomenon about electron lifetime is understandable according to Zaban′s suggestion.[24] In Zaban′s model, which could explain the shape of $\tau'_n \sim V_{OV}$ curve qualitatively, the electron lifetime is mainly affected by the surface state traps in the nanoparticulated TiO_2 film. In OCVD curves, an exponential increase due to internal trapping and detrapping would occur in the middle voltage region. As show in Figure 8, the lifetimes in the middle voltage region (0.2−0.5 V) can be obviously found to decrease in the order of composite electrode containing 10 wt % nanorods, bare P25, and nanorod electrodes. Therefore, it can be concluded that the composite electrode has less surface trap due to the one-dimensional structure of TiO_2 nanorod as compared to the bare P25 electrode. However, the insufficient photoexcited electrons lead to shorter electron lifetime of the bare nanorod electrode owing to its poor dye absorption. This result is consistent with that derived from EIS measurements. For a abare P25 electrode, a lot of grain boundaries would increase the surface trap and reduce the electron lifetime, resulting in relatively low photocurrent and efficiency. Mixing a TiO_2 nanorod to a P25 electrode could decrease the surface trap due to the one-dimensional structure of the nanorods. This is favorable to prolong the electron lifetime and improve the performance of electrode. Nevertheless, the poor dye absorption of nanorods limits the quantity of the photoexcited electron when the content of nanorods in the electrode moves beyond 10 wt % as described above, which leads to short electron lifetime and low photocurrent. Consequently, the composite electrode containing 10 wt % nanorods has the best photovoltaic performance because of its less surface trap and sufficient dye adsorption.

3.4. Overview of the Effect of the Nanorods on Performance of the Solar Cell. The TiO_2 nanorods were also applied as scattering layer (SL) in our case. To investigate the effect of the nanorod scattering layer on DSSCs, one layer scattering TiO_2 nanorods were coated on a bare P25 electrode and the composite electrode containing 10 wt % nanorods. Panels a and b of Figure 9 show the $J-V$ curves of the bare P25 electrode and the composite electrode containing 10 wt % nanorods with and without the nanorod scattering layer, respectively. The results clearly indicate the different functions of nanorod scattering layer on the bare P25 electrode and the composite electrode. As shown in Figure 8a, the performance of the DSSC is improved significantly after adding the nanorod scattering layer. V_{OC}, J_{SC}, FF, and η are increased from 0.66 V, 6.32 mA cm^{-2}, 0.67, and 2.81% to 0.72 V, 7.57 mA cm^{-2}, 0.69, and 3.70%, respectively. However, when the nanorod scattering layer is applied to the composite electrode containing 10 wt % nanorods, as shown in Figure 9b, the performance of the DSSC decreases. V_{OC}, J_{SC}, FF, and η are decreased from 0.69 V, 10.13 mA cm^{-2}, 0.67, and 4.68% to 0.67 V, 8.78 mA cm^{-2}, 0.63, and 3.79%, respectively.

These different behaviors of DSSCs on nanorod layer could be explained by the scattering effect of the TiO_2 nanorods in the composite electrode containing 10 wt % nanorods. As shown in Scheme 1, lots of the incident light in the bare P25 electrode would penetrate the film electrode due to the small size of P25 nanoparticles. This drawback results in great loss of incident light. As scattering layer on the top of the P25 film, the nanorods with larger particle size can reflect back the penetrating light to the P25 electrode, which could enhance the light harvesting efficiency and compensate for loss of the incident light.

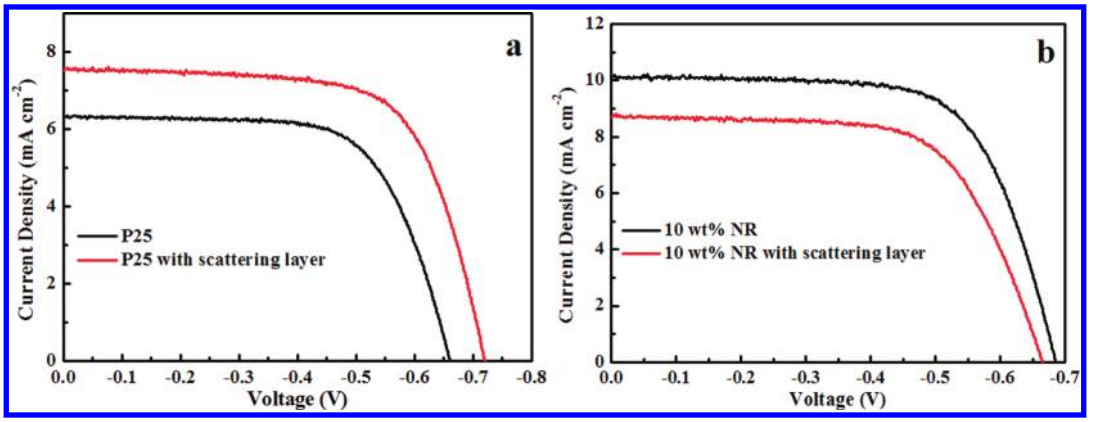

Figure 9. *J*−*V* curves of DSSCs fabricated with the bare P25 electrodes (a) and the composite electrode containing 10 wt % nanorods (b) with and without nanorod scattering layer.

Scheme 1. Scattering Effect of TiO_2 Nanorods on the Bare P25 Electrode and the Composite Electrode Containing 10 wt % Nanorods

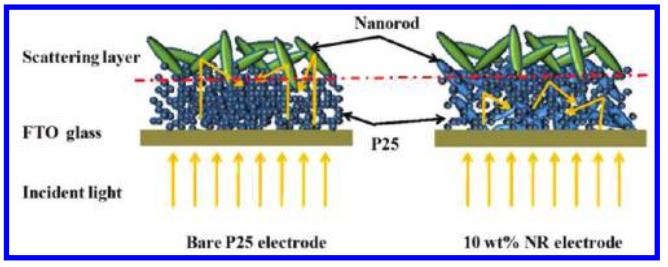

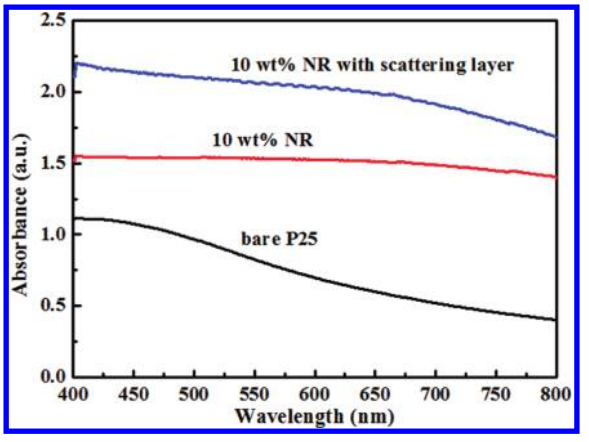

Figure 10. UV−vis measurements of bare P25 film, 10 wt % nanorod film, and 10 wt % nanorod film with scattering layer.

This should be the main reason for the improved performance of the DSSC based on the bare P25 electrode. However, the positive effect of scattering layer does not happen in the composite electrode containing 10 wt % nanorods. Oppositely, the present of nanorod scattering layer lowers the cell performance. It is can be inferred that the TiO_2 nanorod in the underlayer of composite electrode containing 10 wt % nanorods can also reflect the incident light as scattering particles due to their relatively larger particles, most of the penetrating light has been reflected inner the film before reaching the nanorod scattering layer. Figure 10

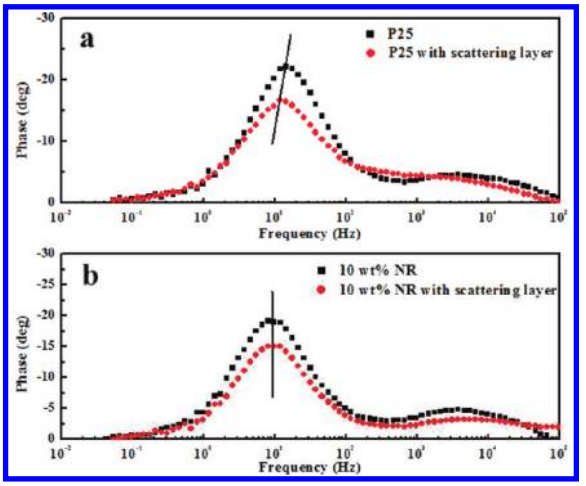

Figure 11. EIS spectra of DSSCs with the bare P25 electrodes (a) and the composite electrode containing 10 wt % nanorods (b) with and without nanorod scattering layer.

shows UV−vis measurements of undyed bare P25 film, 10 wt % nanorod film, and 10 wt % nanorod film with scattering layer. As can be seen, comparing with the bare P25 film, 10 wt % nanorod film exhibits significantly increased absorbance of the UV−vis light, indicating the great scattering effect of the nanorods in 10 wt % nanorod film. At this point, besides the reasons discussed in the section in Figure 4, the scattering effect on the incident light in the composite electrode containing 10 wt % nanorods should be another important reason to improve the performance of DSSCs. After the nanorod scattering layer is added to 10 wt % nanorod film, further growth of absorbance of the UV−vis light is obtained. However, because most of the incident light has been reflected by the nanorods in 10 wt % nanorod film, the nanorod scattering layer on the top of the composite electrode containing 10 wt % nanorods does not contribute greatly to the performance of the cell as the one coated on the bare P25 electrode. Negatively, the nanorod scattering layer increases the film thickness and may enlarge the resistance of the film, which should attribute to the decreased performance of the cell.

Figure 11 illustrates the Bode plots of EIS spectra of the solar cells fabricated with the bare P25 electrodes (a) and the composite electrode containing 10 wt % nanorods (b) with and without the nanorod scattering layer. As for the bare P25

electrode, the peak at the middle frequency region shifts significantly to the lower frequency after adding the nanorod scattering layer, indicating its longer electron lifetime. This should be attributed to the reflection effect of the nanorod scattering layer, which can reduce the loss of penetrating incident light and excite more photoelectrons from dye molecular to the conduction band to get a higher photocurrent and thus prolong the electron lifetime in the film. Nevertheless, the scattering layer for the composite electrode does not show obvious impact on the position of the peak in the middle frequency region. These illustrate that the nanorod scattering layer almost has no evidently positive function on enhancing the photocurrent or prolonging the electron lifetime. Oppositely, the increased thickness of the film coated by the nanorod scattering layer may increase the serial resistance of the cell; this should be the reason for lower performance of the composite electrode containing 10 wt % nanorods with scattering layer. This result also indicates the cell efficiency can be improved without a scattering layer via mixing TiO_2 nanorods to the electrodes in our case.

4. CONCLUSION

Anatase TiO_2 fusiform nanorods are synthesized by a two-step hydrothermal method, and a composite electrode made of the hydrothermally synthesized TiO_2 nanorods and commercial TiO_2 nanoparticles (P25) is proposed for a dye sensitization solar cell. The experimental results show that the above-mentioned composite electrode is an innovative photoanode that can noticeably improve the performances of the solar cell. Under the same fabrication conditions and film thickness, the solar cell made with the composite electrode containing 10 wt % nanorods and 90 wt % P25 nanoparticles demonstrated 66.5% higher device efficiency than that made using bare P25 nanoparticles. Additionally, the nanorods in the electrode can not only provide a straight path for electron transport but also function as scattering particles to increase light harvesting efficiency, which leads to an improvement of efficiency as compared to the cell made with the bare P25 electrode. It should be attributed to the reduced charge recombination and sufficient scattering effect of the nanorods in the electrode. All the results indicate the present TiO_2 nanorod is promising in enhancing the performance of dye-sensitized solar cells.

AUTHOR INFORMATION

Corresponding Author

*E-mail: typeng@whu.edu.cn (T. Y. Peng).

ACKNOWLEDGMENT

This work was supported by the Natural Science Foundation of China (20871096), the Program for New Century Excellent Talents in University (NCET-07-0637), and the Fundamental Research Funds for the Central Universities (2081003) of China.

REFERENCES

(1) O'Regan, B.; Gratzel, M. *Nature* **1991**, *353*, 737–739.
(2) Ito, S.; Nazeeruddin, M. K.; Liska, P.; Comte, P.; Charvet, R.; Pechy, P.; Jirousek, M.; Kay, A.; Zakeeruddin, S. M.; Gratzel, M. *Prog. Photovoltaics* **2006**, *14*, 589–601.
(3) Ito, S.; Liska, P.; Comte, P.; Charvet, R. L.; Pechy, P.; Bach, U.; Schmidt-Mende, L.; Zakeeruddin, S. M.; Kay, A.; Nazeeruddin, M. K.; Gratzel, M. *Chem. Commun.* **2005**, 4351–4353.
(4) Tan, B.; Wu, Y. Y. *J. Phys. Chem. B* **2006**, *110*, 15932–15938.
(5) Lee, J. C.; Kim, T. G.; Lee, W.; Han, S. H.; Sung, Y. M. *Cryst. Growth Des.* **2009**, *9*, 4519–4523.
(6) Adachi, M.; Murata, Y.; Takao, J.; Jiu, J. T.; Sakamoto, M.; Wang, F. M. *J. Am. Chem. Soc.* **2004**, *126*, 14943–14949.
(7) Paulose, M.; Shankar, K.; Varghese, O. K.; Mor, G. K.; Hardin, B.; Grimes, C. A. *Nanotechnology* **2006**, *17*, 1446.
(8) Flores, I. C.; de Freitas, J. N.; Longo, C.; De Paoli, M. A.; Winnischofer, H.; Nogueira, A. F. *J. Photochem. Photobiol., A* **2007**, *189*, 153–160.
(9) Chen, Q. W.; Xu, D. S. *J. Phys. Chem. C* **2009**, *113*, 6310–6314.
(10) Lin, C. J.; Yu, W. Y.; Chien, S. H. *Appl. Phys. Lett.* **2008**, *93*, 133107.
(11) Kokubo, H.; Ding, B.; Naka, T.; Tsuchihira, H.; Shiratori, S. *Nanotechnology* **2007**, *18*, 165604.
(12) Joshi, P.; Zhang, L. F.; Davoux, D.; Zhu, Z. T.; Galipeau, D.; Fong, H.; Qiao, Q. Q. *Energy Environ. Sci.* **2010**, *3*, 1507–1510.
(13) Zhang, Q. F.; Cao, G. Z. *J. Mater. Chem.* **2011**, *21*, 6769–6774.
(14) Hore, S.; Vetter, C.; Kern, R.; Smit, H.; Hinsch, A. *Sol. Energy Mater. Sol. Cells* **2006**, *90*, 1176–1188.
(15) Shin, K.; Jun, Y.; Moon, J. H.; Park, J. H. *ACS Appl. Mater. Interfaces* **2010**, *2*, 288–291.
(16) Ito, S.; Chen, P.; Comte, P.; Nazeeruddin, M. K.; Liska, P.; Pechy, P.; Gratzel, M. *Prog. Photovoltaics* **2007**, *15*, 603–612.
(17) Nian, J. N.; Teng, H. S. *J. Phys. Chem. B* **2006**, *110*, 4193–4198.
(18) Wang, Z. S.; Kawauchi, H.; Kashima, T.; Arakawa, H. *Coord. Chem. Rev.* **2004**, *248*, 1381–1389.
(19) Park, N. G.; van de Lagemaat, J.; Frank, A. J. *J. Phys. Chem. B* **2000**, *104*, 8989–8994.
(20) Li, X.; Lin, H.; Li, J. B.; Li, X. X.; Cui, B.; Zhang, L. Z. *J. Phys. Chem. C* **2008**, *112*, 13744–13753.
(21) Koelsch, M.; Cassaignon, S.; Minh, C. T. T.; Guillemoles, J. F.; Jolivet, J. P. *Thin Solid Films* **2004**, *451−52*, 86–92.
(22) Wang, Q.; Moser, J. E.; Gratzel, M. *J. Phys. Chem. B* **2005**, *109*, 14945–14953.
(23) Zhao, D.; Peng, T. Y.; Lu, L. L.; Cai, P.; Jiang, P.; Bian, Z. Q. *J. Phys. Chem. C* **2008**, *112*, 8486–8494.
(24) Kern, R.; Sastrawan, R.; Ferber, J.; Stangl, R.; Luther, J. *Electrochim. Acta* **2002**, *47*, 4213–4225.
(25) Hoshikawa, T.; Yamada, M.; Kikuchi, R.; Eguchi, K. *J. Electrochem. Soc.* **2005**, *152*, E68–E73.
(26) Murakami, T. N.; Ito, S.; Wang, Q.; Nazeeruddin, M. K.; Bessho, T.; Cesar, I.; Liska, P.; Humphry-Baker, R.; Comte, P.; Pechy, P.; Gratzel, M. *J. Electrochem. Soc.* **2006**, *153*, A2255–A2261.
(27) Bisquert, J.; Zaban, A.; Greenshtein, M.; Mora-Sero, I. *J. Am. Chem. Soc.* **2004**, *126*, 13550–13559.